coatings

MDPI

Article

Enhanced Fracture Toughness of WC-CoCr Thermally Sprayed Coatings by the Addition of NiCrFeSiBC and Mo and Its Influence on Sliding Wear Behavior

José de Jesús Ibarra [1,*], Marco Aurelio González [2], Eduardo Rodríguez [3], Gabriel Israel Vásquez [1], Ariosto Medina [4], José Bernal [5], Claudio Aguilar [6] and Eduardo Enrique Velez [7]

1 TecNM, Instituto Tecnológico José Mario Molina Pasquel y Henríquez, Unidad Académica Zapopan, Camino Arenero No. 1101, Colonia el Bajío, Zapopan 45019, Mexico
2 Centro Universitario de Ciencias Exactas e Ingenierías, CONAHCYT-Universidad de Guadalajara, CUCEI, Ciudad Universitaria, Blvd. Marcelino García Barragán 1421, Guadalajara 44430, Mexico
3 Departamento de Ingeniería de Proyectos, Centro Universitario de Ciencias Exactas e Ingenierías, CUCEI, Universidad de Guadalajara, Ciudad Universitaria, Blvd. Marcelino García Barragán 1421, Guadalajara 44430, Mexico
4 UMSNH, Instituto de Investigación en Metalurgia y Materiales, Edificio U, Ciudad Universitaria, Morelia 58000, Mexico
5 Instituto Tecnológico de Orizaba, Tecnológico Nacional de México, Ote. 9, Emiliano Zapata, Orizaba 94320, Mexico
6 Departamento de Ingeniería Metalúrgica y Materiales, Universidad Técnica Federico Santa María, Valparaíso 2391206, Chile
7 Departamento de Ingeniería Mecánica Eléctrica, Centro Universitario de Ciencias Exactas e Ingenierías, CUCEI, Universidad de Guadalajara, Blvd. Marcelino García Barragán # 1421, Guadalajara 44430, Mexico
* Correspondence: jose.ibarra@zapopan.tecmm.edu.mx

Abstract: Wear is a major issue in industry, particularly with metal components. Therefore, it is crucial to investigate methods that offer increased resistance to this phenomenon. In this research, three coating systems (pure WC-CoCr and WC-CoCr/NiCrFeSiBC+Mo, 88:12 and 83:17 wt.%) were thermally sprayed on an AISI 1018 steel substrate through the High-Velocity Oxygen Fuel (HVOF) process. The coatings were characterized using a field emission scanning electron microscope (FESEM) equipped with the energy dispersive spectroscope (EDS) and X-ray diffractometry (XRD). An analysis of the wear rate for ball-on-flat linear reciprocating sliding tribological tests for the coatings was also carried out. The coating microstructure presents well-dispersed NiCrFeSiBC splats. The WC-CoCr/NiCrFeSiBC+Mo, 88:12, system has the highest wear resistance, decreasing by 30.2% at high loads compared to commercial WC-CoCr CERMETs, and also exhibits the highest fracture toughness. Analysis of wear tracks shows that the material removal at all charges occurred mainly by an abrasive wear mechanism.

Keywords: NiCrFeSiBC; sliding wear; coatings; fracture toughness; WcCoCr; HVOF

Citation: Ibarra, J.d.J.; González, M.A.; Rodríguez, E.; Vásquez, G.I.; Medina, A.; Bernal, J.; Aguilar, C.; Velez, E.E. Enhanced Fracture Toughness of WC-CoCr Thermally Sprayed Coatings by the Addition of NiCrFeSiBC and Mo and Its Influence on Sliding Wear Behavior. *Coatings* **2024**, *14*, 1207. https://doi.org/10.3390/coatings14091207

Academic Editor: Nikolaos Karkalos

Received: 23 August 2024
Revised: 11 September 2024
Accepted: 14 September 2024
Published: 19 September 2024

1. Introduction

In the metal–mechanical industry, the components of any machine are exposed to different types of wear: erosive, abrasive, and sliding [1,2]. In this context, CERMET (ceramic–metallic) coatings have been demonstrated to be an excellent anti-wear option, reducing material loss considerably by this type of damage and increasing the lifespan of the components at a reduced cost of fabrication [3–5]. CERMET commonly consists of hard ceramic particles embedded in a metallic matrix; Tungsten–Carbides WC-Co and WC-CoCr are the most used to refurbish engineering components like, for example, internal gate valves, metal working tools, mining tools, and blast-spray nozzles [6]. Commonly, by using thermal spraying processes such as High-Velocity Oxygen Fuel (HVOF) and Air Plasma Spray, these materials can be applied as coatings [4,7–10]. In this sense, HVOF, it is

well known, can produce more dense coatings due to the influence of its high-speed jet. However, during thermal spraying, a decarburization process occurs invariably, affecting, to some degree, the fracture toughness of the final coating due to the formation of a more brittle carbide W_2C [11–13].

On the other hand, the coatings produced with these compounds have demonstrated excellent resistance under friction wear conditions. Decarburization of W_2C decreases hardness and fracture toughness, promoting greater damage when they experience more severe operating conditions [14–17]. In this context, J. Garcia et al. [14] investigated the relationship between the microstructure and mechanical properties (hardness, modulus of elasticity, and toughness) of systems like WC-Co, SiC, Alumina, satellites, cast iron, and steel. They found that WC-Co coatings showed higher elastic modulus and compressive strength than the other materials. However, their fracture toughness was lower than that observed for cast iron and hardened steels.

Recently, some research has been conducted on enhancing fracture toughness for this type of compound. These investigations include adding reinforcements like carbon nanofibers, mixing them with metallic alloys with higher toughness, or increasing the Co binder [18,19].

Concerning the tribological performance of WC coating CERMETs, Rachidi et al. [20] evaluate the addition of 40% of a metallic alloy to produce a NiCrBSi-60%WC coating. They fabricated their samples using oxyacetylene flame thermal spraying, subjecting them to sand/wheel dry abrasive and continuous motion pin-on-disc wear tests. They concluded that NiCrBSi improves resistance to abrasive wear, and the low fracture toughness of these coatings was one of the factors that promoted the detachment of WC particles through crack propagation.

According to this, producing CERMET mixed coatings with a deformable phase that participates not as a binder alloy but as a different matrix remains challenging. Capable of improving fracture toughness to some extent without sacrificing the hardness considerably. As mentioned above, some functionally graded WC-Co or CoCr/NiCrFeSiBC higher than 20% have been studied and demonstrated an increase in fracture toughness. Still, unfortunately, under friction wear conditions, all coatings displayed lower wear resistance compared with the 100% WC, mainly due to the considerable reduction in hardness. Based on the above, the objective of this project was to produce a composite CERMET/metal coating that possesses better fracture toughness and hardness values close to that displayed by the 100% WC-CoCr coating. As a secondary material matrix, the alloy commercially known as Dimalloy 2001 (NiCrFeBSiC) was used because of its good corrosion resistance. The Molybdenum (Mo) was incorporated into this alloy to improve corrosion resistance and lubricity. Two percentages of a premixed alloy NiCrFeSiBC+Mo (12 and 17 wt.%) were added to the WC-CoCr CERMET to produce corresponding coatings through the HVOF process. Then, they underwent sliding wear tests at three different loads. Also, a detailed description of the interaction and relation of microstructure, hardness, and fracture toughness on wear factors such as wear micro-mechanism is addressed.

2. Materials and Methods

2.1. Materials and Coatings Fabrication

An AISI 1018 steel plate of 50 mm × 40 mm × 7 mm was used as a substrate for coating deposition. Subsequently, surface conditioning was performed through sand-blasting using aluminum oxide as abrasive media (particle size 250–400 μm), obtaining a final average Ra roughness of ~4.5 μm, and applying acetone cleaning to remove remaining organic contaminants and dust. Two powders were used as raw materials, WC-CoCr (Co 10%, C 5.3%, Cr 4.0, W balance) and NiCrFeSiBC+Mo (Cr 16.5%, Fe 4.5%, Si 4.2%, B 3.1%, C 0.8%, Ni balance. + Mo 2%). A 98 (NiCrFeSiBC)-2 (Mo) (wt.%) powder mix was produced through mechanical milling in a planetary ball mill (PQ-N2, Across International), using 8YSZ balls as milling media and with a 1:22 powder: ball ratio at 300 rpm after six hours of milling. Then, a homogeneous modified powder mix of WC-CoCr/NiCrFeSiBC+Mo at 88:12 and

83:12 wt.% concentrations (Figure 1a,b). Then, in the facilities of the company SURESA S.A DE C.V, by using the HVOF thermal spraying process equipped with a Jet Kote gun (See Table 1 for projection parameters), the following coating systems were fabricated: (1) WC-CoCr, (2) WC-CoCr/NiCrFeSiBC+Mo (88:12 wt.%), and (3) WC-CoCr/NiCrFeSiBC+Mo (83:17 wt.%).

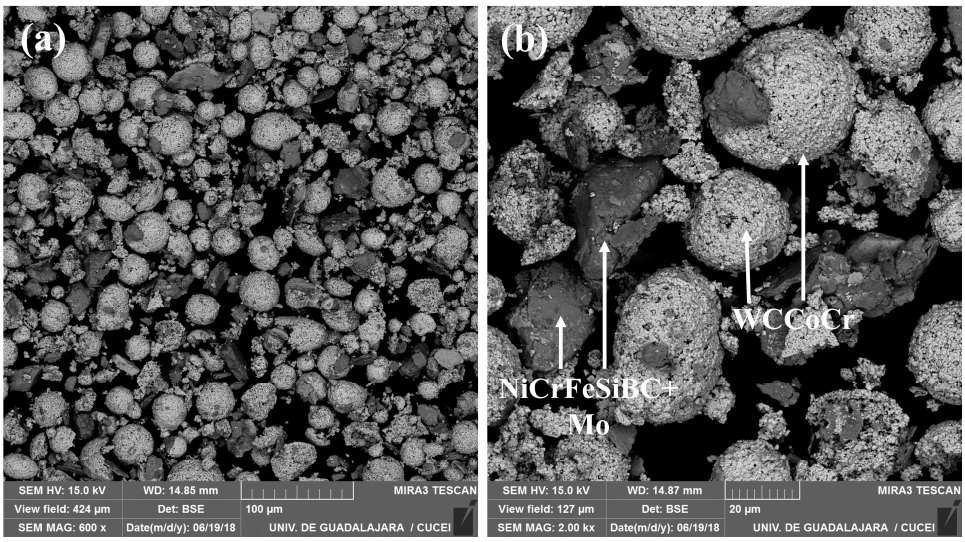

Figure 1. Micrograph of WC-CoCr/NiCrFeSiBC+Mo (83:17 wt.%) feedstock powder, (**a**) Low magnifications (600×), (**b**) High magnifications (2000×).

Table 1. HVOF parameters.

	Hydrogen Pressure (psi)	Oxygen Pressure (psi)	Argon Pressure (psi)	Oxygen Flow (%)	Hydrogen Flow (%)	Spray Distance (mm)	Feed Rate (rpm)
HVOF	110	118	105	60	80	190	3

2.2. Coatings Characterization

The coatings were sectioned, encapsulated in epoxy resin, roughed, and polished using diamond lap films and polish suspension. After metallographic preparation, the samples were placed in an ultrasonic bath (for 10 min for each sample), thus ensuring their cleanliness (eliminating polishing and grinding residues). Then, the identification of the splats corresponding to each powder, their distribution in the coating, and their chemical composition were determined using a Field emission scanning electron microscope (FESEM, Tescan MIRA3 LMU) equipped with a Bruker XFlash 6I30 dispersive energy spectrometer, manufactured by Tescan Group, Kohoutovice Czech Republic. The identification of crystallographic phases was made using an X-ray Panalytical Empyrean diffractometer and the following testing parameters: CuKα radiation (λ = 1.542 Å) at an acceleration potential of 20 kV, a scattering (2θ) angle range from 20° to 90° and a step size of 0.02° (2θ). The microhardness of the coatings was measured on conditioned mirror-polished cross-sections using a Future-Tech FM800 hardness tester manufactured by Future-Tech Corp, Kawasaki, Japan, and by applying a load of 0.5 Kgf. Indentations were obtained using the same apparatus to determine fracture toughness (Equation (1)) by applying a 1 Kgf load and the Palmqvist method [21], which relates the cracks formed in the corners with the indentation diagonals.

$$K_{IC} = 0.0319\left(\frac{P}{a\sqrt{l_a}}\right) \quad (1)$$

where P is the load used during indentation, a is the length of the diagonal from the center to the vertex where the fracture begins, l_a is the result of subtracting the length from the center of the indentation to the end of the crack c minus the length a (see Figure 2).

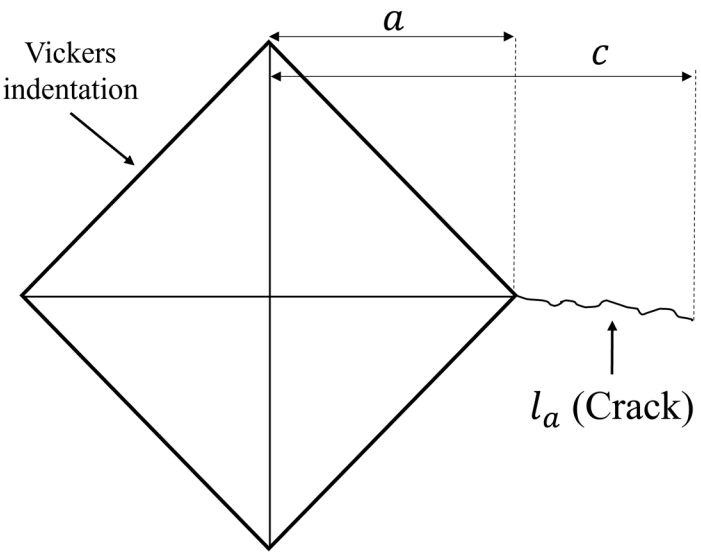

Figure 2. Palmqvist method scheme.

2.3. Sliding Wear Tests

According to ASTM G133-22 [22], tests were carried out. A contact profilometry was used to determine the coupon's average roughness (Ra) before testing, measuring a roughness between 0.02 and 0.05 µm. Subsequently, non-lubricated reciprocating wear tests were carried out at room temperature using a CTR UMT2R tribometer (Bruker, Billerica, MA, USA and applying 10, 30, and 60 N loads with a sliding stroke of 10 mm at a 3 Hz frequency with a total time of 7200 s. Aluminum balls (Al_2O_3) of 5 mm diameter were used as a counterbody. The coefficient of friction was measured in samples at 30 N and 60 N different loads.

2.4. Characterization of Worn Surfaces

The specific wear rate (W) was calculated by measuring the material lost (V) using a Profilm3D optical profilometer. The obtained value is divided by the load (F) and multiplied by the total sliding distance of the test (L) using Equation (2) [20].

$$W = \frac{V}{FL} \quad (2)$$

Finally, all worn surfaces were analyzed through scanning electron microscopy (SEM) to identify and understand the wear mechanisms involved.

3. Results and Discussion

3.1. Microstructure Characterization

Initially, specimens were properly identified, as shown in Table 2, according to their composition and load test. Figure 3a–c shows the coating microstructure of typical WC-CoCr and samples with 12% and 17% NiCrFeSiBC+Mo (dark gray splats), respectively. In addition, a certain percentage of porosity was observed ($\leq$0.43%, see Table 2). In the case of samples B-0 and C-0, the presence of NiCrFeSiBC+Mo was observed in the form of particles or continuous inter-splat films, as shown in Figure 3b,c. Subsequently, to corroborate that the dark gray splats are NiCrFeSiBC+Mo, several EDS analyses were carried out in these regions, and through an EDS spectrum, the presence of these elements could be confirmed, see Figure 3d. The thickness of the coatings was approximately 230 µm.

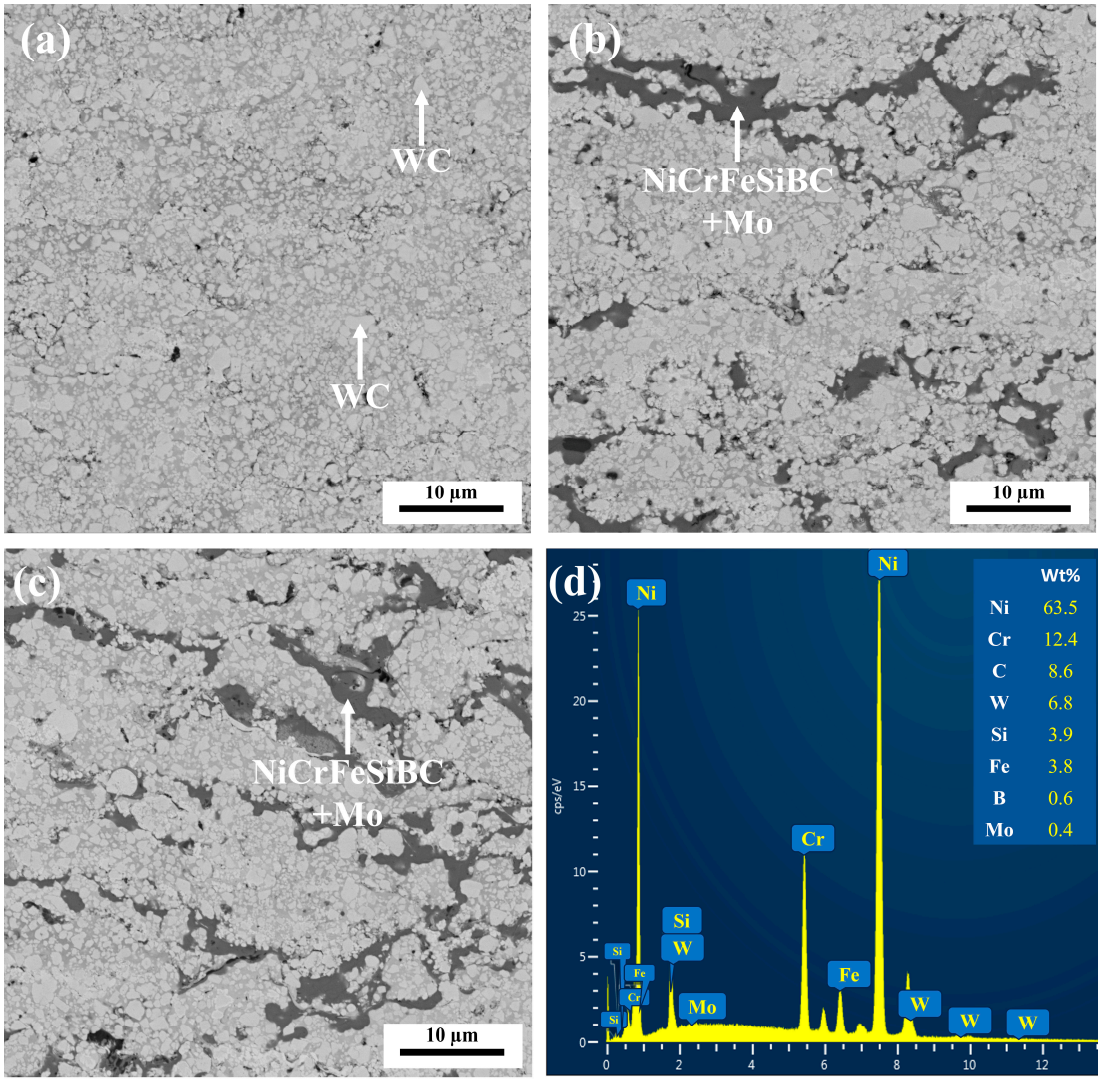

Figure 3. SEM cross-section images of samples: (**a**) A-0, (**b**) B-0, (**c**) C-0, and (**d**) EDS of NiCrFeSiBc+Mo.

Table 2. Specimens identification.

Specimens	Identification	Load (N)	Porosity	Microhardness, HV_{500}	K_{IC} ($MPa \cdot m^{1/2}$)
WC-CoCr	A-0	0	0.43 ± 0.17	1052.06 ± 40.12	12.48 ± 2.52
WC-CoCr and 12% NiCrFeSiBC+Mo	B-0		0.4 ± 0.04	887.04 ± 15.96	15.90 ± 2.83
WC-CoCr and 17% NiCrFeSiBC+Mo	C-0		0.23 ± 0.05	812.82 ± 41.25	13.61 ± 1.34
WC-CoCr	A-10	10			
WC-CoCr and 12% NiCrFeSiBC+Mo	B-10				
WC-CoCr and 17% NiCrFeSiBC+Mo	C-10				
WC-CoCr	A-30	30			
WC-CoCr and 12% NiCrFeSiBC+Mo	B-30				
WC-CoCr and 17% NiCrFeSiBC+Mo	C-30				

Table 2. *Cont.*

Specimens	Identification	Load (N)	Porosity	Microhardness, HV_{500}	K_{IC} ($MPa \cdot m^{1/2}$)
WC-CoCr	A-60	60			
WC-CoCr and 12% NiCrFeSiBC+Mo	B-60				
WC-CoCr and 17% NiCrFeSiBC+Mo	C-60				

Furthermore, Figure 4 shows the phases identified by X-ray diffraction in the sprayed coatings. In the three as-sprayed systems, WC and W_2C were identified [23–25]. During the thermal spraying, decarburization of the WC particles occurred, and the W_2C phase was formed. This process occurs according to the following reaction: $2WC \rightarrow W_2C + C$, the free carbon of this reaction gets oxidized, giving rise to CO or CO_2, which causes the decarburization of the WC particles [23]. In addition, the Co phase can be observed with less intensity [4]. On the other hand, the γ-Ni phase was identified in samples B-0 and C-0 because Ni is the element in the greatest quantity in NiCrBSiC [26,27]. The only notable difference between these two samples is the slight intensity increase in the γ-Ni peak of the C-0 sample.

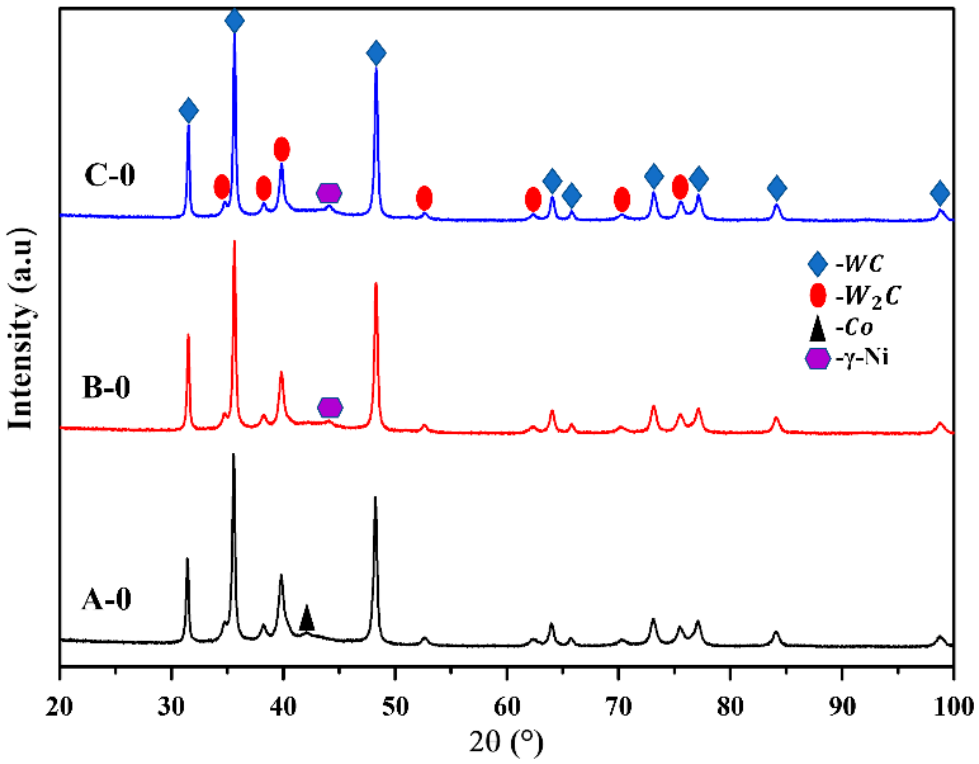

Figure 4. XRD diffractograms of as-sprayed samples.

3.2. Microhardness Fracture Toughness and Sliding Wear

The microhardness values of samples in the as-sprayed condition were measured along the cross-section of the coating microstructures (see Table 2). As expected, the maximum microhardness corresponds to sample A-0 [25,28,29]. It was found that the hardness values for the B-0 and C-0 systems decreased between 15.6% and 22.7%, with an increase in metal binder content of 12% and 17% by weight, respectively. This behavior has been observed in previous studies [27,30]. Some of the factors that influence the hardness of this type of coating are the retained WC phase, the hardness of the binder phase, and the microstructure of the coating (porosity, grain size) [31].

From the results of Table 2, the following is established: the samples with higher hardness (A-0) exhibit a reduction in their fracture toughness property compared to the B-0 and C-0 coatings. The lower number of defects and smaller area of fragile regions due to the dissolution of WC results in greater fracture toughness [31]. The fracture mechanism is governed by the unstable propagation of pre-existing defects that may be inherent to the processing or induced in the formation process [5,6]. Some cracks around each indentation exhibit different lengths and do not form in the corners of the indentations; generally, the state of stresses in these regions is higher. Also, Figure 5 illustrates the representative indentation marks resulting from K_{IC} evaluation in our systems. The upper left insets of Figure 5a–c show how the cracking path occurs, preferably along the WC/Co interface. Regarding the indentations obtained to evaluate the K_{IC}, it is evident that the crack length is shorter in sample B-0 (see Figure 5b), which presented the highest resistance to fracture toughness (K_{IC}), compared to samples A-0 and C-0 (see Figure 5a,c), which exhibit lower resistance.

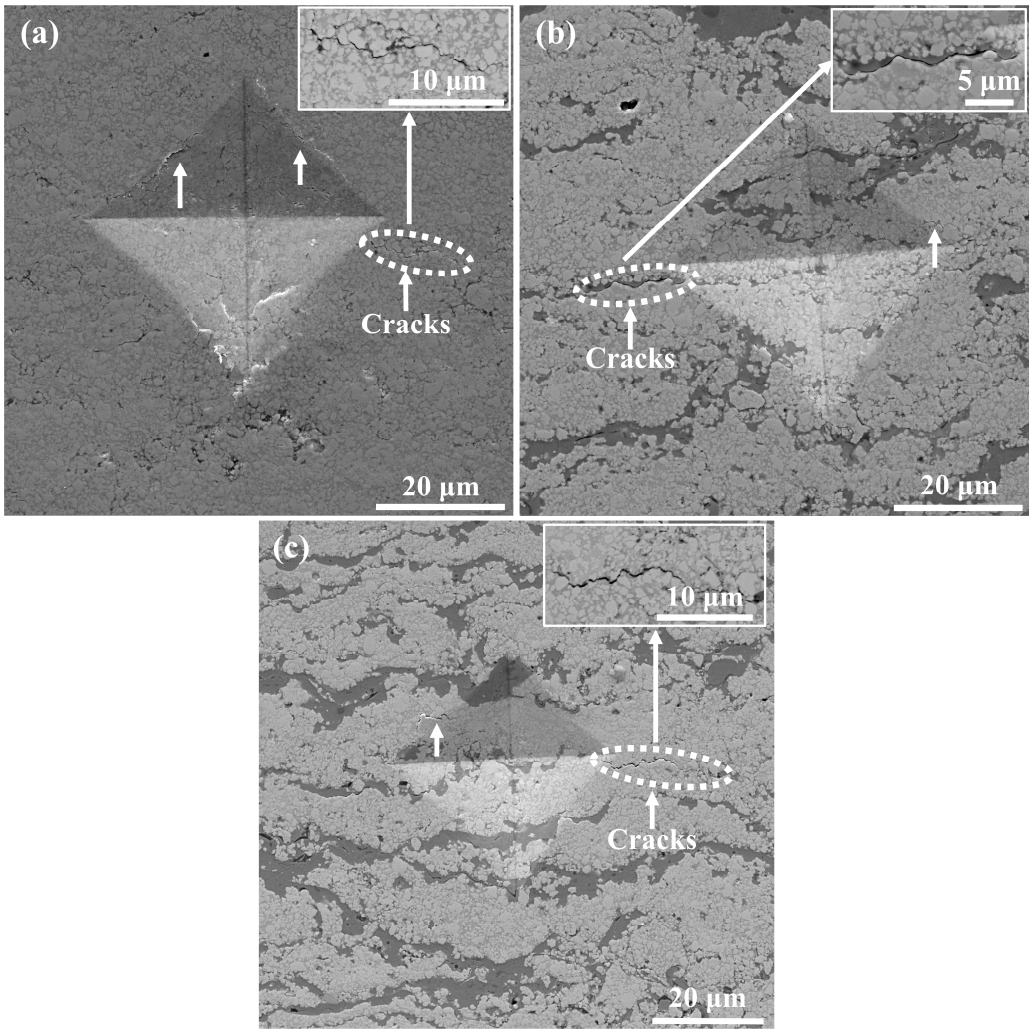

Figure 5. Micrographics of Vickers indentations of samples: (**a**) A-0, (**b**) B-0, and (**c**) C-0.

As a function of the applied load, the specific wear rate for all coating is presented in Figure 6. The average specific wear values remain relatively close for all samples at low loads (10 N), deviating somewhat when subjected to higher loads (i.e., 30 and 60 N). Usually, in brittle materials like ceramics, the rate of material loss caused by fracture is greater than that of plastic deformation [20]. The wear rate of sample B-60 decreased by 30.2% compared to the A-60. The volume wear of a brittle material depends on both

the hardness and fracture toughness of the worn material and on the hardness of the abrasive [32]. Generally, the harder and tougher the matrix is, the lower the wear rate is.

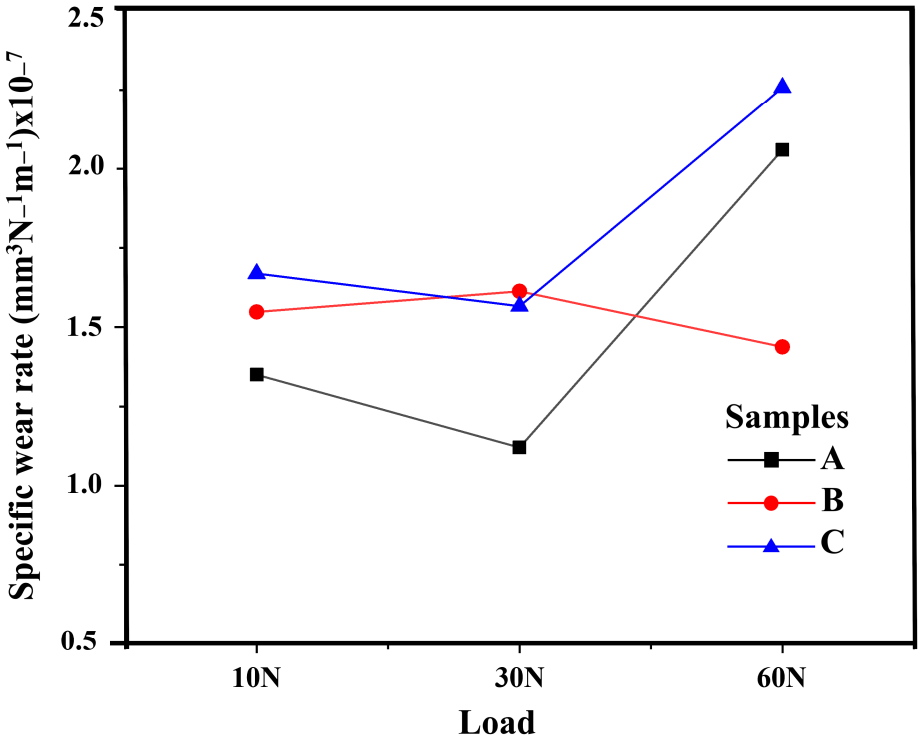

Figure 6. Specific wear rate.

3.3. Coefficient of Friction and Wear Mechanisms

The coefficient of friction was measured on the samples after sliding wear (loads of 30 N and 60 N), and the results are shown in Figure 7. The behavior of the coefficient of friction differs for each system according to the NiCrFeSiBC+Mo content and the load. The most significant coefficient of friction changes occurred at the highest load (60 N); see Figure 7b. Incorporating high NiCrFeSiBC+Mo contents lowers the COF significantly. While at 12%, the high elastic modulus NiCrFeSiBC+Mo particles resist deformation under the high Hertzian contact load. The lowest coefficient of friction observed at higher loads (60 N) is attributed to the formation of a more stable tribolayer directly related to the increase in temperature on the tribo-system; its stability is reflected in the spallation process delay [33]. Therefore, the coating and counter body's wear mechanism may differ.

The oxidation of elemental species within the test couples leads to the formation of tribo-films [28]. The oxidation process occurs due to the ignition temperature during the asperity interaction in the sliding contact. In WC-Co coatings on sliding contacts, the formation of tribo-films of WO_3 and CoO caused by the isothermal oxidation of WC-Co or even $WCoO_4$ at higher temperatures (~200–300 °C) has been reported [28,34]. In this regard, the formation of $CoWO_4$ and WO_3 on the worn surface of the coatings acts as a solid lubricant and reduces the friction coefficient [30,35]. Furthermore, the brittle fracture mechanism increases friction forces by providing an additional mechanism for energy dissipation in the test regions [30]. The above counteracts the lubricating effect of the oxides formed by the tribochemical processes.

SEM micrographs of the wear traces produced from the sliding wear tests are shown in Figure 8. Small pores can be visible on the worn surface mainly in samples A-30, A-60, and C-60 (see red circles in Figure 8d,g,i), likely to be sites where material pullout of WC occurred. According to the above, with a load of 60 N in the test, systems A-60 and C-60 experience greater porosity and a greater rate of wear. In this sense, stresses concentrate in the material in areas of porosity, resulting in cracks propagating from these

areas [30]. This process is evidenced in samples A-30, C-30, and A-60 (see inserts of Figure 8d,g). Mechanisms of wear in samples are shown in Figure 8. The worn surfaces showed agglomeration of debris particles and parallel grooves in the sliding direction (induced by a detachment of debris particles trapped in the contact surface due to sliding). The main reason is the shear stress that resulted from normal load and friction force on the contact surface.

The presence of these visible grooves on the worn surface, formed by the passage of harder material through softer areas of the microstructure, suggests that the wear mechanism in all systems was abrasive wear. The adhesion strength between splats is further weakened due to the defects (such as porosity and micro-crack) appearing mostly on the boundaries between thin oxide sheets and splats. Later, the fatigue damage accumulates to a certain value, and micro-cracks initiate at the defects between splats. Micro-cracks grow and propagate, leading to the spallation of the splats. Thus, wear debris is generated (see inserts in Figure 8, which shows the fracture mechanism, transgranular in samples A-30, C-30, and A-60, while in B-60, the mechanism is intergranular, see yellow circles).

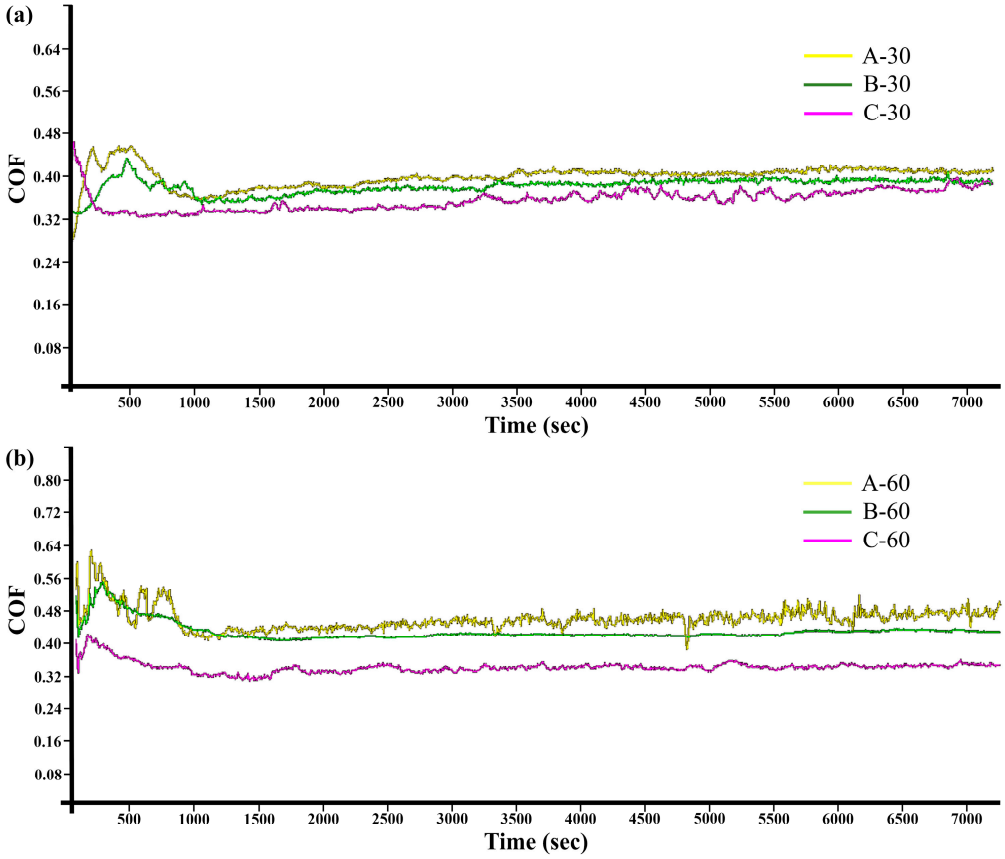

Figure 7. Coefficient of friction of samples at different loads, (**a**) 30 N and (**b**) 60 N.

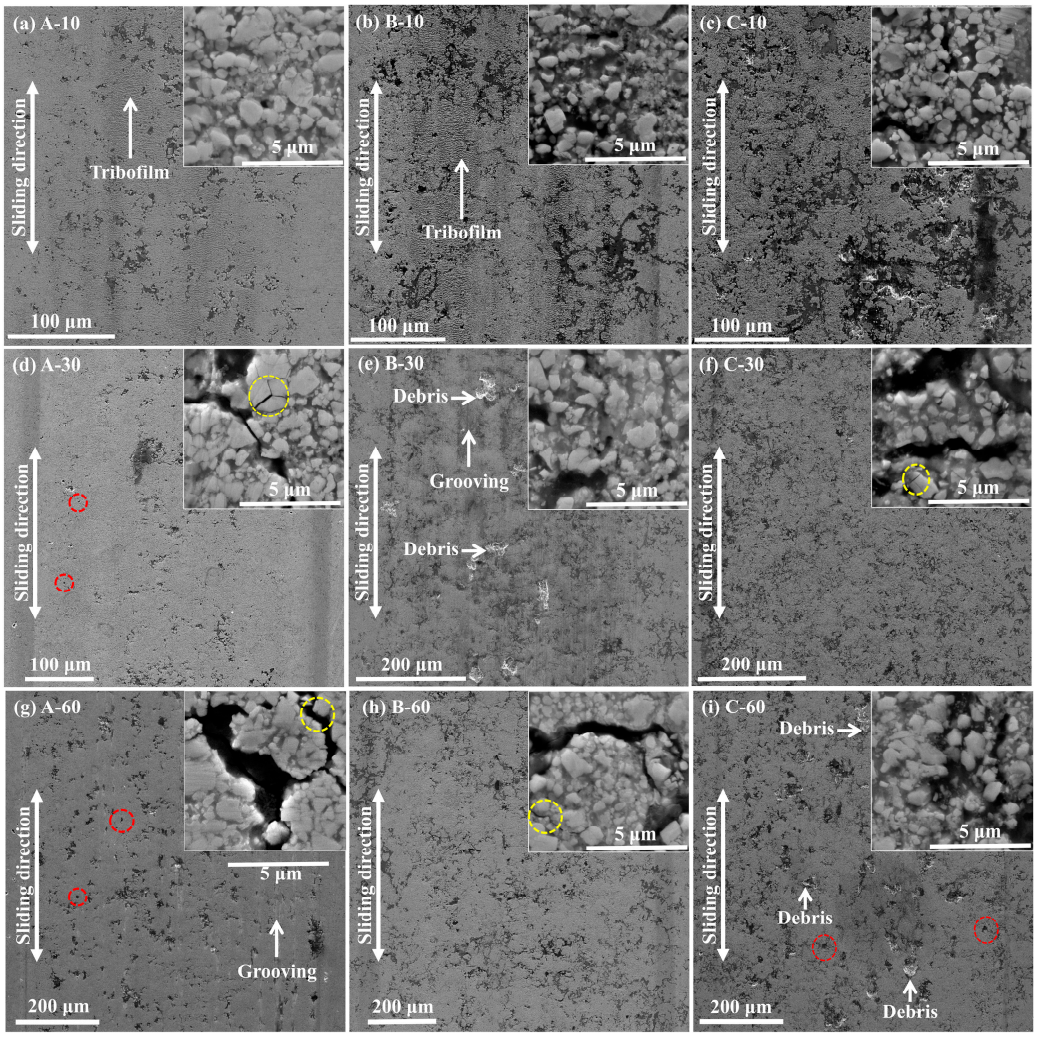

Figure 8. Mechanisms of wear, (**a**–**c**), (**d**–**f**), (**g**–**i**) corresponding to A, B, and C samples, respectively.

4. Conclusions

The present work demonstrated that adding 12% NiCrFeSiBC+Mo to commercial WC-CoCr CERMETS would be beneficial because the specific wear rate at higher loads (60 N) was decreased by approximately 30.2% (maintaining high hardness).

The highest resistance to fracture toughness also occurs in coatings with the adhesion of 12% NiCrFeSiBC+Mo, which is directly related to the higher wear resistance.

There is a decrease in the coefficient of friction when adhering to the WC-CoCr CERMETS (NiCrFeSiBC+Mo) in both percentages (12 and 17%) and is attributed to the formation of a more stable tribolayer directly related to the increase in temperature on the tribo-system, its stability is reflected in the spallation process delay.

Author Contributions: Conceptualization, J.d.J.I., M.A.G. and E.R.; methodology, J.d.J.I., C.A. and G.I.V.; validation, J.d.J.I., C.A. and M.A.G.; formal analysis, J.d.J.I., M.A.G. and E.R.; investigation, J.d.J.I., M.A.G. and E.E.V.; resources, M.A.G., E.R. and A.M.; data curation, G.I.V., J.B. and A.M.; writing—original draft preparation, J.d.J.I., M.A.G. and E.R.; writing—review and editing, E.R., G.I.V. and M.A.G.; visualization, G.I.V., J.B. and A.M.; supervision, J.B., E.E.V. and C.A.; project administration, J.d.J.I., M.A.G. and E.R.; funding acquisition, M.A.G., E.R. and J.d.J.I. All authors have read and agreed to the published version of the manuscript.

Funding: This research received no external funding.

Institutional Review Board Statement: Not applicable.

Informed Consent Statement: Not applicable.

Data Availability Statement: The data supporting this study's findings are available from the corresponding author upon reasonable request.

Acknowledgments: The authors thank the CONAHCYT, the Universidad de Guadalajara, and the Instituto Tecnológico José Mario Molina Pasquel y Henriquez for the technical support, and the SURESA S.A DE C.V company, Tonala, Mexico, for the deposition of the coatings.

Conflicts of Interest: The authors declare no conflicts of interest.

References

1. Ibarra, J.; Rodríguez, E.; González, M.A.; Cuenca, S.L.; Medina, A.; Vásquez, G.I. Erosion Behavior of 440C Stainless Steel Cryogenically Treated. *Rev. Mex. Ing. Quim.* **2020**, *19*, 1255–1264. [CrossRef]
2. Plucknett, K.P.; Jin, C.; Onuoha, C.C.; Stewart, T.L.; Memarrashidi, Z. The Sliding Wear Response of High-Performance Cermets. In *Handbook of Mechanics of Materials*; Springer: Singapore, 2018; pp. 1–42.
3. Zhang, S. Titanium Carbonitride-Based Cermets: Processes and Properties. *Mater. Sci. Eng.* **1993**, *163*, 141–148. [CrossRef]
4. González, M.A.; Rodríguez, E.; Mojardín, E.; Jiménez, O.; Guillen, H.; Ibarra, J. Study of the Erosive Wear Behaviour of Cryogenically and Tempered WC-CoCr Coating Deposited by HVOF. *Wear* **2017**, *376–377*, 595–607. [CrossRef]
5. Katranidis, V.; Kamnis, S.; Allcock, B.; Gu, S. Effects and Interplays of Spray Angle and Stand-off Distance on the Sliding Wear Behavior of HVOF WC-17Co Coatings. *J. Therm. Spray Technol.* **2019**, *28*, 514–534. [CrossRef]
6. Bolleddu, V.; Racherla, V.; Bandyopadhyay, P.P. Comparative Study of Air Plasma Sprayed and High Velocity Oxy-Fuel Sprayed Nanostructured WC-17wt%Co Coatings. *Int. J. Adv. Manuf. Technol.* **2016**, *84*, 1601–1613. [CrossRef]
7. Bravo, S.; Torres-González, J.; Morales-Hernández, J.; Martínez-Franco, E.; González-Olvera, J.C.; Mercader-Trejo, F.E.; Rodríguez-López, A.; Manzano-Ramírez, A.; Esparza, A.; Herrera-Basurto, R. Effect of the Manufacturing Parameters on the Quality of the Ceramic Thermal Barrier Coating after Ageing by Thermal Treatment. *Rev. Mex. Ing. Quim.* **2021**, *20*, 227–237. [CrossRef]
8. Zhou, Y.K.; Kang, J.J.; Yue, W.; Fu, Z.Q.; Zhu, L.N.; She, D.S. Wet Sliding Wear of HVOF-Sprayed WC-10Co4Cr Coatings in Simulated Seawater Drilling Fluid. *J. Therm. Spray Technol.* **2021**, *30*, 2174–2186. [CrossRef]
9. Gerner, D.; Azarmi, F.; McDonnell, M.; Okeke, U. Application of Machine Learning for Optimization of HVOF Process Parameters. *J. Therm. Spray Technol.* **2024**, *33*, 504–514. [CrossRef]
10. Federici, M.; Straffelini, G.; Gialanella, S. Pin-on-Disc Testing of Low-Metallic Friction Material Sliding Against HVOF Coated Cast Iron: Modelling of the Contact Temperature Evolution. *Tribol. Lett.* **2017**, *65*, 1–12. [CrossRef]
11. Yuan, J.; Zhan, Q.; Huang, J.; Ding, S.; Li, H. Decarburization Mechanisms of WC-Co during Thermal Spraying: Insights from Controlled Carbon Loss and Microstructure Characterization. *Mater. Chem. Phys.* **2013**, *142*, 165–171. [CrossRef]
12. Mazaheri, Y.; Khodaveysi, E.; Roknian, M.; Sheikhi, M.; Heidarpour, A. 75Cr_3C_2-25NiCr and 86WC-10Co-4Cr High Wear- and Corrosion-Resistant Cermet Coatings Deposited on A356 Substrate by High-Velocity Oxy-Fuel Technique. *Coatings* **2022**, *12*, 1408. [CrossRef]
13. Wang, X.; Xing, Z. Preparation and Properties of Composite Nanoceramic NiCrBSi-TiO_2/WC(Co) Coatings. *Coatings* **2020**, *10*, 868. [CrossRef]
14. García, J.; Collado Ciprés, V.; Blomqvist, A.; Kaplan, B. Cemented Carbide Microstructures: A Review. *Int. J. Refract. Met. Hard. Mater.* **2019**, *80*, 40–68. [CrossRef]
15. Ahmed, R.; Vourlias, G.; Algoburi, A.; Vogiatzis, C.; Chaliampalias, D.; Skolianos, S.; Berger, L.M.; Paul, S.; Faisal, N.H.; Toma, F.L.; et al. Comparative Study of Corrosion Performance of HVOF-Sprayed Coatings Produced Using Conventional and Suspension WC-Co Feedstock. *J. Therm. Spray Technol.* **2018**, *27*, 1579–1593. [CrossRef]
16. Uzun, A.; Altuncu, E.; Ustel, F.; Turk, A.; Ozturk, S. Investigation of Wear Behaviour of HVOF Sprayed WC-Co Coatings for Automotive Parts in Different Working Conditions. *Int. J. Surf. Sci. Eng.* **2011**, *5*, 180–192. [CrossRef]
17. Stoica, V.; Ahmed, R.; Golshan, M.; Tobe, S. Sliding Wear Evaluation of Hot Isostatically Pressed Thermal Spray Cermet Coatings. *J. Therm. Spray Technol.* **2004**, *13*, 93–107. [CrossRef]
18. Pasha, M.; Kaleemulla, M. Erosive Wear Behavior of Sprayed Metal Matrix Composites: An Overview. *Proc. Inst. Mech. Eng. Part J J. Eng. Tribol.* **2013**, *227*, 1063–1075. [CrossRef]
19. Sharma, M.; Goyal, K.; Kaushal, G.; Goyal, D.K.; Scholar, R. Erosive Behaviour of HVOF Sprayed Coatings: A Review 1. *Int. J. Eng. Sci.* **2017**, *63019*, 219–243.
20. Rachidi, R.; Kihel, B.E.; Delaunois, F.; Vitry, V.; Deschuyteneer, D. Wear Performance of Thermally Sprayed NiCrBSi and NiCrBSi-WC Coatings under Two Different Wear Modes. *J. Mater. Environ. Sci.* **2017**, *8*, 4550–4559. [CrossRef]
21. Spiegler, R.; Schmauder, S.; Sigl, L.S. Fracture Toughness Evaluation of WC Co Alloys by Indentation Testing. *J. Hard Mater.* **1990**, *1*, 147–158.
22. *ASTM G133-22*; Standar Test Method for Linearly Reciprocating Ball-on-Flat Sliding Wear. ASTM International: West Conshohocken, PA, USA, 2022; pp. 1–6.
23. Shu, W.; Deng, X.; Guo, W.; Shi, W.; Li, S.; Zhang, B.; Bai, J.; Cui, Q. Microstructure and Wear Resistance of HVOF Sprayed WC-10Co-4Cr Coating on Ti-6Al-4V. *Heat Treat. Surf. Eng.* **2022**, *4*, 70–75. [CrossRef]

24. Xie, Z.; Zhang, C.; Wang, R.; Li, D.; Zhang, Y.; Li, G.; Lu, X. Microstructure and Wear Resistance of WC/Co-Based Coating on Copper by Plasma Cladding. *J. Mater. Res. Technol.* **2021**, *15*, 821–833. [CrossRef]
25. Pulsford, J.; Venturi, F.; Pala, Z.; Kamnis, S.; Hussain, T. Application of HVOF WC-Co-Cr Coatings on the Internal Surface of Small Cylinders: Effect of Internal Diameter on the Wear Resistance. *Wear* **2019**, *432–433*, 202965. [CrossRef]
26. Buytoz, S.; Ulutan, M.; Islak, S.; Kurt, B.; Nuri Çelik, O. Microstructural and Wear Characteristics of High Velocity Oxygen Fuel (HVOF) Sprayed NiCrBSi-SiC Composite Coating on SAE 1030 Steel. *Arab. J. Sci. Eng.* **2013**, *38*, 1481–1491. [CrossRef]
27. Psyllaki, P.; Vardavoulias, M.; Kekes, D.; Psyllaki, P.; Vardavoulias, M. Wear Micro-Mechanisms of Composite WC- Co/Cr-NiCrFeBSiC Coatings. Part I: Dry Sliding. *Tribol. Ind.* **2014**, *36*, 361–374.
28. Ahmed, R.; Ali, O.; Berndt, C.C.; Fardan, A. Sliding Wear of Conventional and Suspension Sprayed Nanocomposite WC-Co Coatings: An Invited Review. *J. Therm. Spray Technol.* **2021**, *30*, 800–861. [CrossRef]
29. Bergant, Z.; Batič, B.Š.; Felde, I.; Šturm, R.; Sedlaček, M. Tribological Properties of Solid Solution Strengthened Laser Cladded NiCrBSi/WC-12Co Metal Matrix Composite Coatings. *Materials* **2022**, *15*, 342. [CrossRef]
30. Pulsford, J.; Venturi, F.; Kamnis, S.; Hussain, T. Sliding Wear Behaviour of WC-Co Reinforced NiCrFeSiB HVOAF Thermal Spray Coatings against WC-Co and Al_2O_3 Counterbodies. *Surf. Coat. Technol.* **2020**, *386*, 125468. [CrossRef]
31. Nahvi, S.M.; Jafari, M. Microstructural and Mechanical Properties of Advanced HVOF-Sprayed WC-Based Cermet Coatings. *Surf. Coat. Technol.* **2016**, *286*, 95–102. [CrossRef]
32. Sun, L.; Pan, J.; Lin, C. Wear Behavior of TiC-$MoSi_2$ Composites. *Mater. Lett.* **2003**, *57*, 1239–1243. [CrossRef]
33. García-León, R.A.; Martínez-Trinidad, J.; Campos-Silva, I.; Figueroa-López, U.; Guevara-Morales, A. Wear Maps of Borided AISI 316L Steel under Ball-on-Flat Dry Sliding Conditions. *Mater. Lett.* **2021**, *282*, 128842. [CrossRef]
34. Yang, Q.; Senda, T.; Hirose, A. Sliding Wear Behavior of WC-12% Co Coatings at Elevated Temperatures. *Surf. Coat. Technol.* **2006**, *200*, 4208–4212. [CrossRef]
35. Guilemany, J.M.; Miguel, J.M.; Vizcaino, S.; Climent, F. Role of Three-Body Abrasion Wear in the Sliding Wear Behaviour of WCCo Coatings Obtained by Thermal Spraying. *Surf. Coat. Technol.* **2001**, *140*, 141–146. [CrossRef]